Precision Engineering 54 (2018) 107–117

Contents lists available at ScienceDirect

Precision Engineering

journal homepage: www.elsevier.com/locate/precision

Measurement of the X-ray computed tomography instrument geometry by minimization of reprojection errors—Implementation on experimental data☆

Massimiliano Ferrucci[a,b,*], Petr Heřmánek[c], Evelina Ametova[a], Elia Sbettega[c], Michal Vopalensky[d], Ivana Kumpová[d], Daniel Vavřík[d], Simone Carmignato[c], Tom Craeghs[b], Wim Dewulf[a]

[a] Mechanical Engineering Department, KU Leuven, 3000, Leuven, Belgium
[b] Research and Development, Materialise NV, 3001, Leuven, Belgium
[c] Department of Management and Engineering, University of Padova, 36100, Vicenza, Italy
[d] Institute of Theoretical and Applied Mechanics, Centre of Excellence Telč, Czech Republic

ARTICLE INFO

Keywords:
X-ray computed tomography
Dimensional metrology
Instrument alignment

ABSTRACT

A procedure for measuring the geometry of X-ray computed tomography (CT) instruments is applied to an experimental CT instrument. In this study, the geometrical measurement procedure is implemented with the CT^2 reference object, comprising steel spheres with known center positions in a local coordinate frame affixed to a cylindrical carbon fiber framework. The procedure can be implemented with other sphere-based reference objects, provided the sphere center coordinates are known. The effects of number of acquired projections and rotation mode (stepped or continuous) on the quality of measured geometrical parameters are studied. Finally, the output of the geometrical measurement procedure is used to inform the physical adjustment of the experimental CT instrument to its ideal alignment. The effectiveness of the measurement procedure to correctly determine the instrument geometry is demonstrated from dimensional measurements performed on a tomographically reconstructed validation object from radiographs acquired under initial (misaligned) and adjusted (aligned) instrument geometry.

1. Introduction

The geometry of an X-ray computed tomography (CT) instrument is defined by the relative positions and orientations of the three major components: X-ray source focal spot, sample rotation axis, and detector. Discrepancies between the geometry of the CT instrument with which radiographic projection images are acquired and the backprojection geometry in tomographic reconstruction from the images will contribute to inconsistencies between dimensional measurements performed on the reconstructed volume and the actual dimensions on the measured part(s) [1]. Consequently, these inconsistencies will result in errors of measurements performed on the volumetric data. The ability to measure the geometry of a real CT instrument and subsequent compensation of any detected misalignments is a critical step in improving the quality of reconstructed datasets and in reducing errors in CT measurements [2].

In this study, we apply a geometrical measurement procedure with a dedicated reference object to the TORATOM (Twinned ORthogonal Adjustable TOMograph, see Ref. [3]) experimental CT instrument at the Centre of Excellence Telč, Institute of Theoretical and Applied Mechanics, v.v.i, Czech Academy of Sciences (henceforth referred to by the abbreviation CET). The geometrical measurement procedure is based on the least squares estimation of a set of geometrical parameters in a CT ray-tracing model. The development of the reference object (named the Computed Tomography Calibration Tube—CT^2) is presented in Ref. [4], while the geometrical measurement procedure is introduced and applied to simulated data in Ref. [5]. It should be noted that the geometrical measurement procedure can be implemented with any other sphere-based reference object, provided the sphere center positions in a local coordinate frame are known, e.g. from measurement by CMM. Certain considerations in the practical implementation of this procedure, namely the number of acquired radiographic projection images and the modality with which the reference object is rotated (i.e. stepped or continuous), are investigated to provide an indication of robustness

☆ This paper was recommended by Associate Editor Andreas Archenti.

* Corresponding author. Mechanical Engineering Department, KU Leuven, 3000, Leuven, Belgium.
E-mail address: massimiliano.ferrucci@kuleuven.be (M. Ferrucci).

https://doi.org/10.1016/j.precisioneng.2018.05.007
Received 8 February 2018; Received in revised form 30 March 2018; Accepted 18 May 2018
Available online 25 May 2018

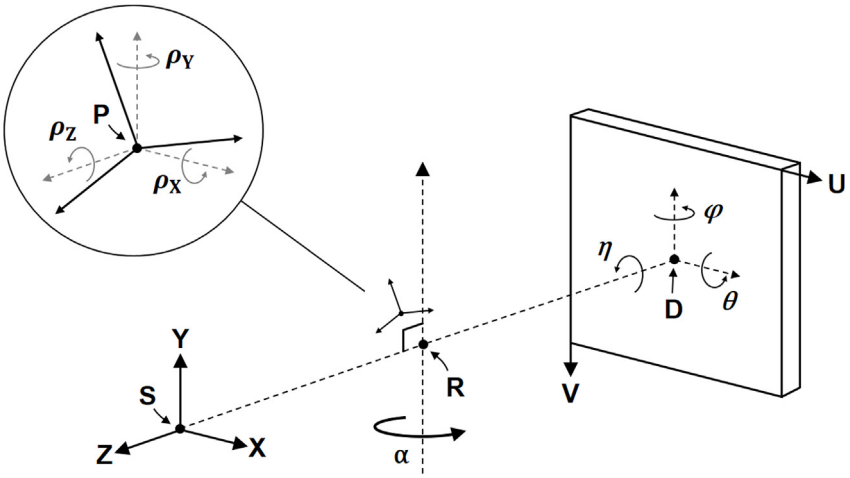

Fig. 1. Scheme for the parameterization of a typical cone-beam CT instrument and the position and orientation of a reference object within the global coordinate frame.

in the measurement of the instrument geometry.

The geometry of the experimental instrument aligned roughly with a standard TORATOM procedure (henceforth referred to as the 'initial' instrument geometry) is measured. Misalignments in the initial geometry are reduced by applying a series of physical adjustments to bring the instrument to its aligned state, which is defined in section 2. CT measurements of a separate validation object are performed under initial and adjusted geometries. Dimensional measurements from both reconstructed datasets are compared to determine the efficacy of the geometrical measurement procedure to correctly inform the physical adjustment of the instrument to its aligned state.

2. Cone-beam CT geometry

The geometry of a cone-beam CT instrument is defined by the relative position and orientation of X-ray source focal spot, axis of object rotation (AOR), and detector [1]. The following description of the coordinate convention is supplemented by the diagram in Fig. 1, which also includes the parameterization of the reference object position and orientation. Coordinate conventions in this study are chosen to correspond to previously used conventions [5]. A right-handed global Cartesian coordinate system is fixed on the X-ray source focal spot. The Y axis is parallel to the AOR, while the Z axis is coincident with the line from the source focal spot **S** that intersects the AOR orthogonally. The X axis subsequently follows the right-hand screw rule. In an aligned instrument, the detector rows are parallel to the global X axis, while the detector columns are parallel to the Y axis. The Z axis ideally intersects the detector at its geometrical center. The U and V axes of the detector coordinate frame correspond to the indexing axes for the detector column and rows, respectively.

The position of the AOR is given by $\mathbf{R} = (0,0, z_R)$, corresponding to the coordinate position of its intersection with the Z axis. The orientation of the AOR is given by the unit vector $\hat{\boldsymbol{r}} = (0,1,0)$. Rotation of the sample stage is parameterized by the angle α. The position of the detector center is parameterized by the point $\mathbf{D} = (x_D, y_D, z_D)$. Detector orientation is defined by three extrinsic rotations performed about local axes that are parallel to the axes of the coordinate system and whose origin is the detector center: tilt θ about the local X-axis, slant ϕ about the local Y-axis, and skew η about the local Z-axis. Rotations are applied in the following order: (1) η, (2) ϕ, and (3) θ.

When measuring the CT geometry, the position and orientation of the reference object must also be determined. Parameterization of the reference object in the CT geometry is given by the position of its local origin and the orientation of its local axes with respect to the global origin and coordinate axes, respectively, at the $\alpha = 0°$ position of the rotation stage. The position of the local origin in the global frame is given by the point $\mathbf{P} = (x_P, y_P, z_P)$ and the orientation of the local axes is given by three extrinsic rotations, performed sequentially in the order (1) ρ_Y, (2) ρ_Z, and (3) ρ_X. These parameters are considered nuisance parameters as they do not describe the CT geometry, yet are necessary for its measurement. The CT geometry can therefore be defined by 13 geometrical parameters: 7 instrument parameters and 6 reference object parameters, summarized in Table 1.

3. Reference object

The reference object presented in Ref. [4] is used in this experimental study and is briefly discussed here. It should be noted that the geometrical measurement procedure, which is described in more detail in Ref. [5], can be implemented with any sphere-based reference object. The CT^2 reference object consists of $M = 48$ high X-ray absorption spheres of 2.5 mm diameter fixed to a hollow, cylindrical carbon fiber support (Fig. 2). Carbon fiber is chosen as the support material due its relatively low X-ray absorption, providing high contrast in the radiographic imaging of the spheres for visual detection. The spheres are arranged in 10 circular trajectories at various heights along the central axis of the cylindrical support. An additional marking sphere is included in the top circular trajectory to break the symmetry and facilitate sphere identification in the radiographs. Sphere locations were chosen to reduce the number of overlaps in their cone-beam projections at the highest magnification position of the reference object while ensuring the full inclusion of all spheres in the detector field of view. The three-dimensional (x, y, z) coordinate position of each sphere center m was measured on a tactile CMM with a maximum permissible error (MPE) of 2 + L/300 μm, where L is the measured length in mm. The set of sphere center coordinates in the object's local frame $(x, y, z)_{m=1,2,\ldots,48}$ constitute the dimensional reference for measurement of the CT geometrical parameters.

Table 1
Geometrical parameters for CT instrument and reference object.

Component	Feature	Parameters
X-ray focal spot	Position	$\mathbf{S} = (0,0,0)$
AOR	Position	$\mathbf{R} = (0,0, z_R)$
AOR	Orientation	$\hat{\boldsymbol{r}} = (0,1,0)$
Detector	Position	$\mathbf{D} = (x_D, y_D, z_D)$
Detector	Orientation	(η, φ, θ)
Reference object	Position	$\mathbf{P} = (x_P, y_P, z_P)_{\alpha=0°}$
Reference object	Orientation	$(\rho_X, \rho_Y, \rho_Z)_{\alpha=0°}$

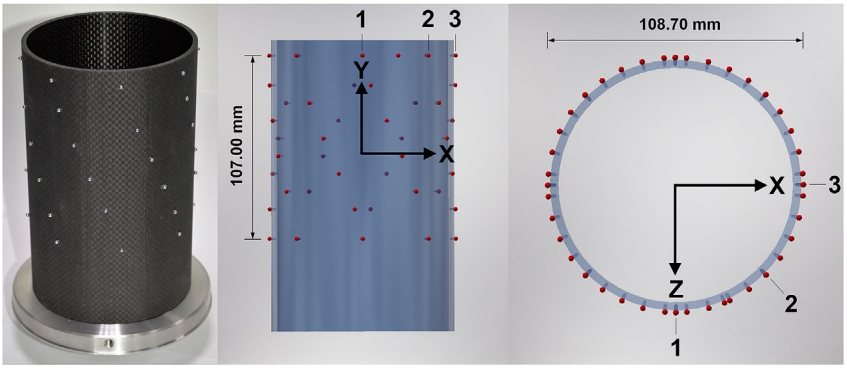

Fig. 2. The Computed Tomography Calibration Tube (CT^2) and local coordinate frame. Spheres are arranged in 10 circular trajectories along the outer circumference of a carbon fiber support.

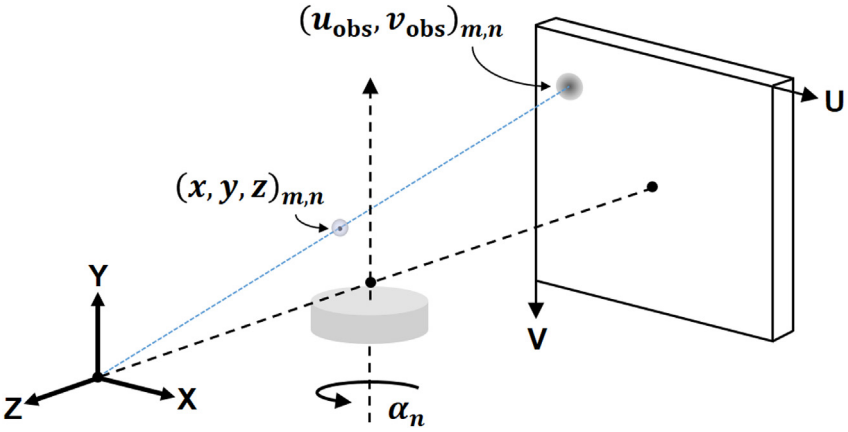

Fig. 3. A ray-tracing operator calculates a set of center projection coordinates given the calibrated sphere center coordinates and the 13 geometrical parameters described in section 2.

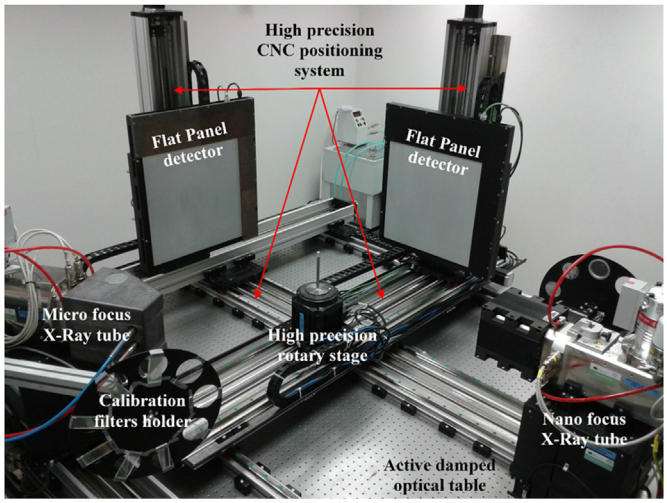

Fig. 4. The TORATOM (Twinned ORthogonal Adjustable TOMograph) experimental CT instrument.

4. Geometrical measurement procedure

Measurement of the CT instrument geometry typically involves taking several radiographs of a reference object and deducing the instrument geometry from subsequent analyses on the projection images [2]. The mathematical analysis can be either analytical or numerical in nature. Analytical methods consist of solving a set of equations relating dimensional features on the reference object and their physical locations on the projection images to the parameters describing the geometry of the imaging system. Numerical methods consist of minimizing the sum of the residuals between modelled and observed sphere center projection coordinates, known as the reprojection error, in the radiographic acquisition of the reference object; henceforth, numerical methods shall be referred to as 'minimization'. Unlike analytical methods, minimization does not require precise a priori knowledge of the position or orientation of the reference object in the instrument coordinate frame. In this study, the global minimization technique described in Ref. [5] is applied and is briefly described below.

The reference object is placed on the sample rotation stage such that the object cylindrical axis is reasonably parallel to and coincident with the axis of rotation. Projection images of the reference object are acquired at $n = 1,2, \ldots, N$ equally-spaced (not necessarily but preferably) rotation positions of the sample stage; the optimal number of images N is discussed in section 6. The settings of the imaging system, e.g. X-ray power, detector sensitivity and exposure time, and pre-filtering, are chosen to maximize contrast in the imaged spheres. Within each acquired radiographic image, the coordinates of each projected sphere center (u_{obs}, v_{obs}) are estimated from the center of an ellipse fitted to the edge of the projected sphere. An enhanced method for estimating the center projection coordinates is presented in Ref. [6] and consists of applying a correction to the ellipse center using the lengths of the major and minor axes of the fit ellipse.

However, the carbon fiber support of the reference object reduces contrast in the edges of the projected spheres, thereby reducing the effectiveness of the correction. Simply using the ellipse center for estimating the center projection coordinates was found to be the most robust method for this particular reference object [5]. Applying this image analysis step to all radiographic images produces a set of

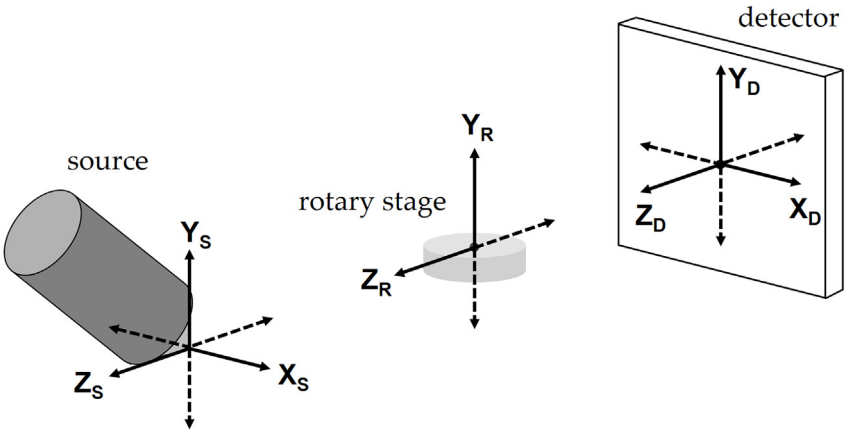

Fig. 5. Kinematic positioning of the X-ray source, rotary stage, and flat-panel detector for the utilized X-ray imaging structure on the TORATOM CT instrument at CET.

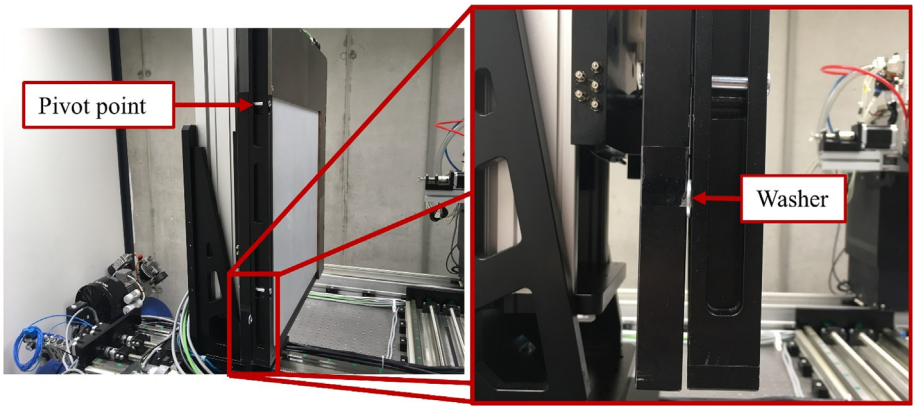

Fig. 6. Modification of the detector orientation by inserting metal washers.

Table 2
Solved instrument geometrical parameters for various numbers of stepped projections of the reference object.

#Proj.	x_D /mm	y_D /mm	z_D /mm	z_R /mm	θ /°	φ /°	η /°
2	0.0532	−0.5200	−1214.7514	−400.9991	0.2510	0.0850	−0.1079
5	0.0500	−0.4780	−1214.5483	−400.9489	0.2391	0.0821	−0.1070
10	0.0503	−0.4633	−1214.5484	−400.9518	0.2405	0.0814	−0.1069
15	0.0506	−0.4554	−1214.5575	−400.9550	0.2412	0.0810	−0.1068
30	0.0510	−0.4509	−1214.5439	−400.9513	0.2411	0.0803	−0.1068
45	0.0511	−0.4503	−1214.5441	−400.9514	0.2408	0.0801	−0.1068
90	0.0512	−0.4488	−1214.5418	−400.9507	0.2407	0.0800	−0.1068
180	0.0511	−0.4490	−1214.5489	−400.9531	0.2410	0.0795	−0.1068
360	0.0511	−0.4491	−1214.5482	−400.9531	0.2409	0.0795	−0.1068
720	0.0511	−0.4488	−1214.5480	−400.9530	0.2409	0.0793	−0.1068
1440	0.0512	−0.4483	−1214.5468	−400.9527	0.2410	0.0794	−0.1068
2880	0.0512	−0.4482	−1214.5464	−400.9526	0.2410	0.0793	−0.1068

observed center projection coordinates $(u_{obs}, v_{obs})_{m,n}$ for each sphere m at each rotation position n of the sample stage.

A ray-tracing operator provides a set of modelled center projection coordinates $(u_{mod}, v_{mod})_{m,n}$ for all angular positions of the sample stage α_n, where $n = 1,2, ...,N$, given a set of 13 initial geometrical parameter values $(p_{initial})_{i=1,2,...,13}$ and the CMM measured sphere center coordinates $(x, y, z)_{m=1,2,...,48}$ at the $\alpha = 0°$ rotation stage position (Fig. 3). The sum of the squared residuals (SSR) between corresponding modelled and observed center projection coordinates, shown in equation (1), is known as the reprojection error and is a measure for the goodness of fit between the modelled and experimental geometries. It should be noted that reprojection error can take other algebraic forms, for example keeping the U and V components of the center projection residuals separate prior to summing instead of summing in quadrature. The implications of other objective functions on the performance of the minimization is a topic of further research. Solving for the geometrical parameters of the experimental instrument, and reference object position and orientation consists of minimizing the reprojection error by iteratively modifying the values of the geometrical parameters in the modelled forward projection operator. Assuming robust implementation of the mathematical problem, the set of solved parameters $(p_{solved})_{i=1,2,...,13}$ in the model that yield the minimum reprojection error should be approximately equal to the actual geometry of the experimental instrument.

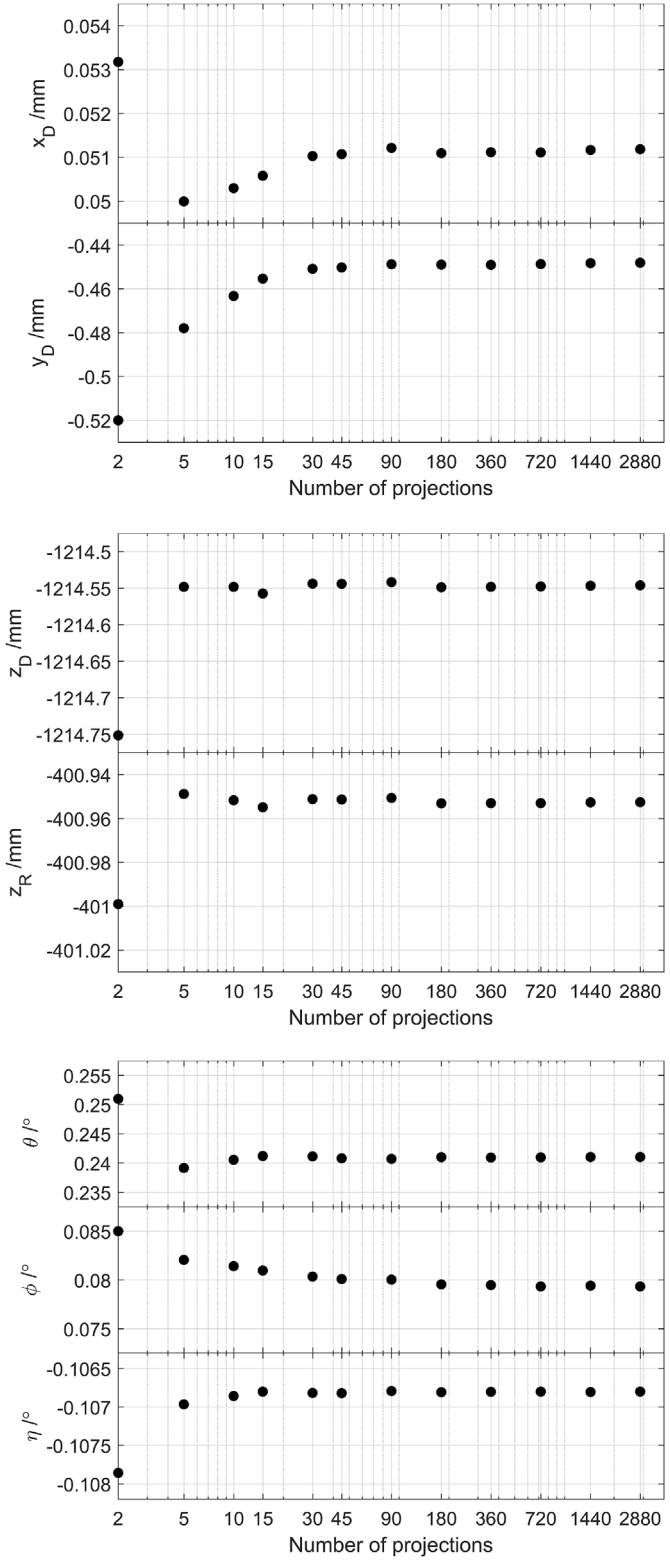

Fig. 7. Comparison of solved instrument geometrical parameters for various numbers of stepped projections. Top: Detector lateral positions x_D and y_D. Center: Detector longitudinal position z_D and rotary stage position z_R. Bottom: Detector orientation θ, φ, and η. Plot horizontal axes are logarithmic for better visualization of results.

Table 3
Comparison of reprojection error 2.5% quantiles ($U_{2.5\%}$ and $V_{2.5\%}$) and 97.5% quantiles ($U_{97.5\%}$ and $V_{97.5\%}$) for various numbers of stepped projections. All values are in pixels.

# Proj.	$U_{2.5\%}$	$U_{97.5\%}$	$V_{2.5\%}$	$V_{97.5\%}$
2	−0.1254	0.1632	−0.0820	0.1269
5	−0.1763	0.1692	−0.1204	0.1381
10	−0.1801	0.1728	−0.1241	0.1334
15	−0.1760	0.1771	−0.1259	0.1313
30	−0.2051	0.1781	−0.1271	0.1237
45	−0.2049	0.1770	−0.1311	0.1300
90	−0.2094	0.1734	−0.1277	0.1251
180	−0.2110	0.1740	−0.1274	0.1245
360	−0.2095	0.1746	−0.1265	0.1234
720	−0.2104	0.1757	−0.1265	0.1243
1440	−0.2112	0.1762	−0.1266	0.1240
2880	−0.2116	0.1767	−0.1265	0.1243

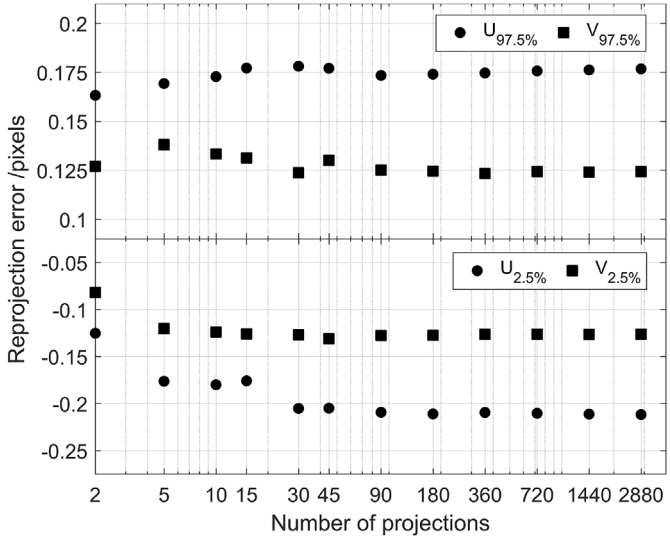

Fig. 8. Reprojection error quantiles plotted as a function of number of stepped projections. Top: 2.5% quantiles ($U_{2.5\%}$) and 97.5% quantiles ($U_{97.5\%}$) for U coordinate reprojection error. Bottom: 2.5% quantiles ($V_{2.5\%}$) and 97.5% quantiles ($V_{97.5\%}$) for V coordinate reprojection error.

$$\sum_{n=1}^{N}\sum_{m=1}^{M}\left(\sqrt{(u_{\mathrm{mod}}(m,n)-u_{\mathrm{obs}}(m,n))^2+(v_{\mathrm{mod}}(m,n)-v_{\mathrm{obs}}(m,n))^2}\right)^2 \tag{1}$$

Each center projection coordinate within each radiographic image constitutes a data point that is used for solving the minimization problem. Therefore, radiographic acquisition and subsequent center projection estimation produces a set of 48 × N center projection coordinates $(u_{\mathrm{obs}}, v_{\mathrm{obs}})_{m,n}$. However, depending on the object position and orientation, overlaps in the projected spheres can occur for a few percent of the total data points and can introduce errors in the estimated center projection coordinates. Therefore, data points corresponding to overlapping spheres are not considered in the minimization problem.

Given the set of M × N observed center projection coordinates $(u_{\mathrm{obs}}, v_{\mathrm{obs}})$, the set of M × N sphere center coordinate positions at all rotation angles (x, y, z), and the initial set of 13 geometrical parameters p_{initial}, the procedure for finding the set of 13 parameters p_{solved} that minimize the reprojection error from equation (1) is performed. MATLAB built-in solver for constrained non-linear minimization is used in conjunction with global optimization tool *GlobalSearch* [7] to reduce the possibility of solving to local minima.

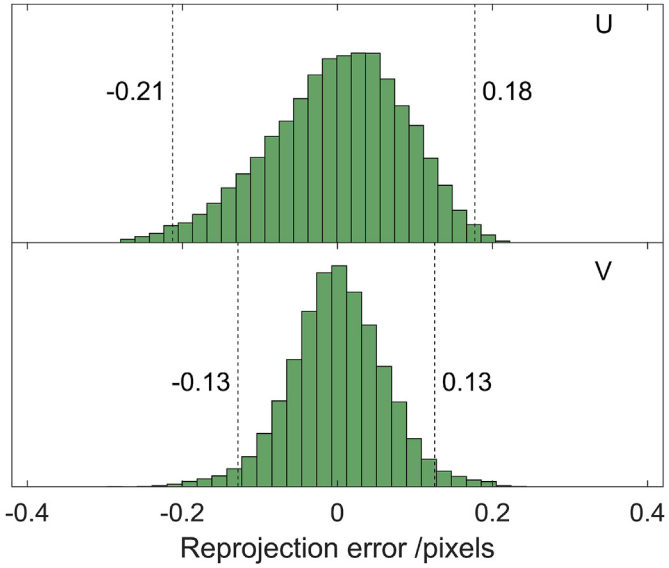

Fig. 9. Reprojection error histograms for acquisition of 720 stepped projections of the reference object. Top: Reprojection errors in U coordinate. Bottom: Reprojection errors in V coordinate. The 95% confidence intervals are shown by dotted lines, corresponding to the 2.5% and 97.5% quantiles.

5. CT instrument

The TORATOM CT instrument at the CET (Fig. 4) is a patented, multi-purpose device comprising two orthogonal, independent X-ray imaging structures. Each structure consists of its own X-ray source and detector. An Aerotech APR150DR rotary stage (Aerotech Inc., USA) is shared by both structures. In this study, only one of the X-ray imaging structures was used, so only its technical specifications are provided. More information on the complete TORATOM CT instrument is given in Ref. [3]. The utilized X-ray imaging structure is equipped with an X-ray WorX XWT-240-SE (X-RAY WorX GmbH, Germany) X-ray source operated for all measurement tasks at 100 kV maximum tube acceleration voltage. Filament current was set to 400 μA for the tests in section 6 and 380 μA for the tests in section 7. A Perkin Elmer XRD1622 (Perkin Elmer Inc., USA) flat-panel detector with Gadolinium oxysulfide (Gadox) scintillator is used to acquire radiographic images. The detector consists of a 2048 × 2048 array of square pixels, each 200 μm in size (side lengths). For all measurements, radiographs were acquired with 1000 ms (1 s) exposures for the tests in section 6 and 1200 ms (1.2 s) exposures for the tests in section 7. Effects due to non-uniformities in the imaging system, for example in the intensity of the emitted beam and in the pixel response, and detector noise are reduced by flat-field correction (see, e.g. Ref. [8]), implemented after acquiring all projections.

Positioning of the instrument components is controlled by way of separate kinematic systems (Fig. 5). The positions of X-ray source and detector can be adapted along three directions in their local Cartesian coordinate axes, while the rotary stage can be positioned along the longitudinal axis between the source and detector and along its vertical Y_R direction. Note that, in the case of a misaligned instrument, the longitudinal axis does not coincide with the magnification axis. Transverse positioning of the detector, i.e. along X_D and Y_D, and X-ray source position along X_S can be adjusted in increments of 1 μm, while positioning of the other axes can be adjusted in increments of < 10 μm. The longitudinal (Z_R) position of the rotary stage, approximately corresponding to the source-to-rotation axis distance (SRD), was chosen to maximize the coverage of the projected reference object in the detector field of view. The position of the rotary stage was kept fixed throughout the experiments in order to avoid positioning errors.

While the in-plane rotation of the detector (η) can be controlled by a stepper motor, the system does not have motorized units for controlling out-of-plane rotations of the detector (φ and θ). Therefore, in order to change the slant and tilt of the detector, metal washers of a specific thickness were placed between the detector and its mount at a certain distance from a pivot point. An example of modifying the detector tilt θ is shown in Fig. 6.

The alignment procedure currently implemented at CET consists of placing a metal rod of known diameter on the rotary stage and acquiring radiographic images. The rotary stage is then moved to a second position along the longitudinal direction and the procedure is repeated. Analysis of the acquired radiographs provides estimates for the CT instrument geometry, namely rotary stage position, detector position, and in-plane rotation of the detector.

6. Robustness testing

Generally, the robustness of a solution to a mathematical problem can be improved by increasing the number of input data points [9]. In this minimization problem, the number of data points can be increased by increasing the number of spheres in the reference object, decreasing the number of projected sphere overlaps, and increasing the number of rotation positions of the sample stage at which radiographic projections of the reference object are acquired. The number of spheres in the CT^2 reference object was maximized while also ensuring minimal occurrence of overlaps in the sphere projections. This means that, for the current reference object, only increasing the number of radiographic

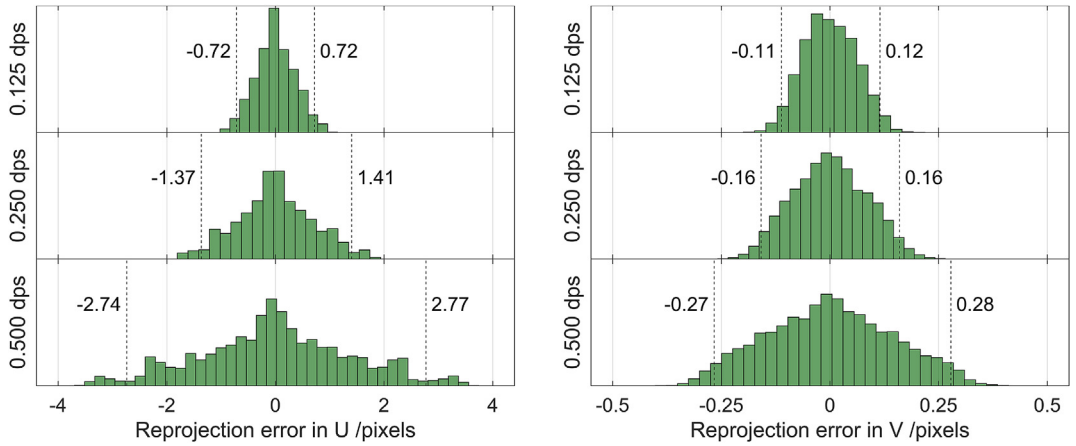

Fig. 10. Histograms of reprojection errors for three continuous rotation speeds: 0.125, 0.25, and 0.5° per second. Left: Reprojection errors in U coordinate. Right: Reprojection errors in V coordinate. The 95% confidence intervals are shown by dotted lines, corresponding to the 2.5% and 97.5% quantiles.

Table 4
Solved CT geometrical parameters from 720 projections of the reference object acquired with three continuous rotation speeds: 0.125, 0.250, 0.500° per second. The solved parameters from stepped acquisition of 720 projections are provided for comparison and change from stepped is shown in percent within the parentheses. The range of solved parameters from continuous rotation is also shown.

Speed/°·s^{-1}	x_D/mm	y_D/mm	z_D/mm	z_R/mm	θ/°	φ/°	η/°
Stepped	0.0511	−0.4488	−1214.5480	−400.9530	0.2409	0.0793	−0.1068
0.125	0.0711	−0.4576	−1214.5557	−400.9608	0.2425	0.0785	−0.1126
	(39.1%)	(2.0%)	(< 0.1%)	(< 0.1%)	(0.7%)	(1.0%)	(5.4%)
0.250	0.0606	−0.4553	−1214.6186	−400.9837	0.2420	0.0798	−0.1175
	(18.6%)	(1.4%)	(< 0.1%)	(< 0.1%)	(0.5%)	(0.6%)	(10.0%)
0.500	0.0687	−0.4496	−1214.5854	−400.9682	0.2418	0.0795	−0.1272
	(34.4%)	(0.2%)	(< 0.1%)	(< 0.1%)	(0.4%)	(0.3%)	(19.1%)
Range	0.0105	0.0080	0.0629	0.0228	0.0007	0.0014	0.0146

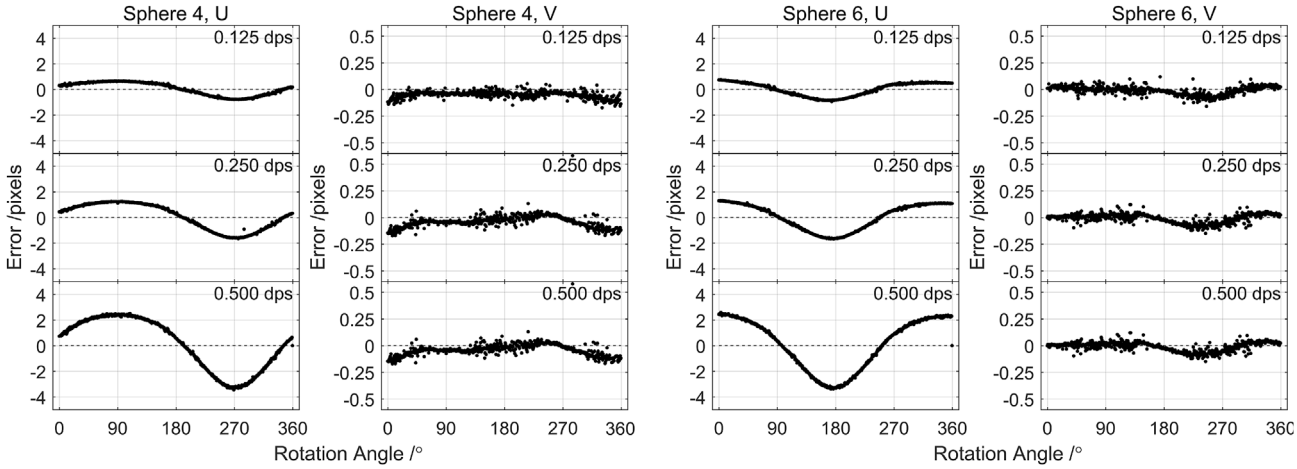

Fig. 11. Error between minimized and observed center projection coordinates for sphere 4 (left) and sphere 6 (right) at three continuous rotation speeds: 0.125, 0.25, and 0.5° per second. Sphere 4 is closest to the detector at rotation angle 90° and closest to the X-ray source at rotation angle 270°. Sphere 6 is closest to the detector at 0° and closest to the X-ray source at 180°.

projections will provide a larger number of data points. However, the time required for acquisition and subsequent processing of radiographs will also increase with more radiographs.

Rotation of the reference object during radiographic acquisition can be either stepped or continuous. In stepped rotation, radiographs are acquired while the sample stage is stopped at the corresponding rotation angle. In continuous rotation, the stage is continuously rotating during data acquisition. Data acquisition by stepped rotation typically takes more time than the same data acquisition with continuous rotation. Furthermore, some rotation stages can exhibit larger angular indexing errors in stepped rotation than in continuous rotation. However, acquiring projections while the stage is continuously rotating can introduce blur in the imaged features, particularly when the rotation results in lateral motion of the feature with respect to the detector plane, i.e. not towards or away from the detector plane; these effects worsen with longer exposures of the detector. In this section, the robustness of the geometrical measurement procedure is tested with respect to the number of acquired radiographs and to the rotation mode.

6.1. Number of projections

There can be a certain number of acquired projections of the reference object, above which the robustness of the geometrical measurement is not improved. In this case, any additional projections of the reference object would not contribute to a more accurate estimation of geometrical parameters and would only increase time and effort for the user. Geometrical measurement was performed on the initial instrument geometry using various numbers of stepped angular positions of the reference object; a minimum of two projections is necessary to solve for rotary stage position z_R. The solved geometrical parameter values are presented for each acquisition in Table 2 and in Fig. 7. Solved parameters for 5 or more projections were relatively consistent. The plots in Fig. 7 show that most results begin to diverge for acquisitions below 30 projections. Furthermore, the coupling between Z positions of rotation axis and detector discussed in Ref. [5] is also present in these experimental results, as shown by the simultaneous increase or decrease in solved values for both variables in Fig. 7, center.

The distribution of reprojection errors, i.e. errors between modelled and observed sphere center projection coordinates, over all data points (all projected spheres at all projections) can also provide an indication of the robustness of the measurement procedure. In Table 3, 95% of the observed reprojection errors are presented by the 2.5% and 97.5% quantiles, corresponding to the lower and upper bounds of the coverage interval, respectively, for each acquisition. Reprojection errors are presented separately for each projected sphere center coordinate in Fig. 8: $U_{2.5\%}$ and $U_{97.5\%}$ correspond to the 2.5% and 97.5% quantiles, respectively, for the horizontal (U) coordinate, while $V_{2.5\%}$ and $V_{97.5\%}$ correspond to the 2.5% and 97.5% quantiles, respectively, for the vertical (V) coordinate. Histograms of the U and V coordinate reprojection errors from the 720 projection acquisition are presented in Fig. 9; this plot will serve as a reference for the reprojection error histograms from continuous rotation (Fig. 10). Dotted vertical lines in the histogram plots denote the lower and upper bounds corresponding to the 2.5% and 97.5% quantiles, respectively, containing 95% of the reprojection error values.

Using at least 5 projections resulted in small differences of the solved parameters, indicating the robustness of the geometrical measurement procedure. Lower reprojection errors for fewer projections could be a result of the smaller sample size and not necessarily an indication that the corresponding solved parameters are more robust.

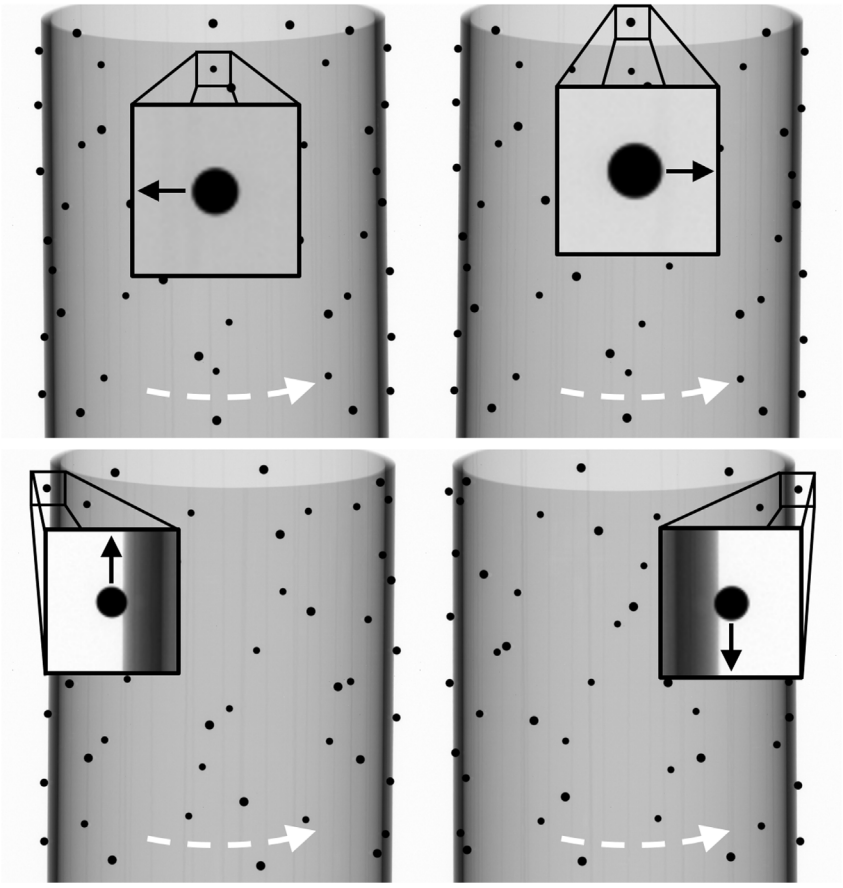

Fig. 12. (Top) The largest errors in the U coordinate of the observed center projection occur when the sphere is closest to the source and, to a lesser extent, when the sphere is closest to the detector. (Bottom) The largest errors in the V coordinate of the observed center projection occur when the sphere motion is either towards or away from the detector, which corresponds to the sphere being at its furthest extent from the detector central column. Dashed arrows indicate direction of stage rotation.

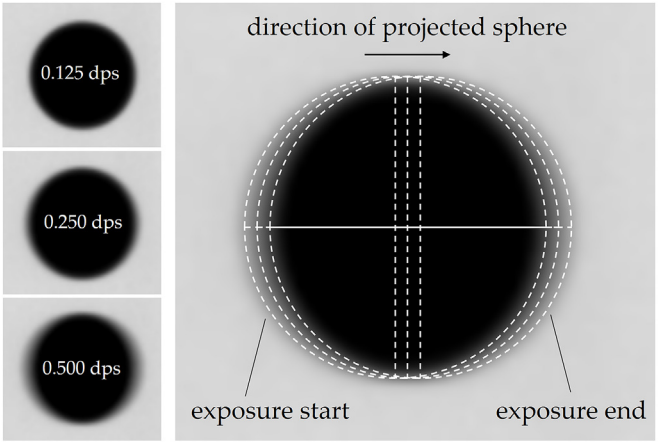

Fig. 13. Under continuous rotation, the projected spheres exhibit increased blur, particularly when they are positioned closest to and furthest from the detector. At these locations, the lateral movement of the sphere with respect to the detector plane is highest. Left: magnified views of projected sphere 6 are shown for the three continuous rotation speeds. Right: the resulting offset between observed and modelled center projection coordinates is due to the continuous movement of the projected sphere from its indexed position in the model, which corresponds to the start of the exposure.

6.2. Continuous rotation

The effects of rotation mode are investigated for three speeds of continuous rotation: 0.125, 0.25, and 0.5° per second. For each rotation speed, 720 projections of the reference object are acquired. Solved parameter values from minimization applied to the radiographs of the reference object acquired under continuous rotation are presented in Table 4. The values from the 720-projection stepped acquisition are included for comparison. Change between continuous and stepped solved values is shown as percent in the parentheses. The largest relative deviations occur for x_D and η. No discernible trend, e.g. divergent parameter values, is observed as a function of rotation speed. Coupling between the Z positions of rotary axis and detector is present in the data from continuous rotation, as is indicated by the simultaneous increase or decrease in the solved values of both variables.

Table 5
Variation in solved initial (rotation position $\alpha = 0°$) orientation of the reference object about the Y axis ρ_Y due to changing speed of continuous rotation.

	Speed of continuous rotation		
	0.125 dps	0.250 dps	0.500 dps
$\rho_Y/°$	0.4453	0.7319	0.9553

Histograms for the reprojection errors under continuous rotation of the reference object are presented in Fig. 13. Dotted vertical lines in the histogram plots denote the lower and upper bounds corresponding to the 2.5% and 97.5% quantiles, respectively, containing 95% of the reprojection error values. Center projection errors under continuous rotation are larger than the center projection errors in stepped acquisition and increase with speed of rotation, which is particularly noticeable for the horizontal (U) coordinate errors.

A systematic behavior is observed when plotting center projection errors for spheres 4 and 6 as a function of rotation angle for each continuous rotation speed (Fig. 11). The largest errors in horizontal U pixel coordinate occur when the sphere is closest to the source and, to a lesser extent, when the sphere is closest to the detector (Fig. 12, top). These locations correspond to the motion of the sphere being almost entirely horizontal with respect to the detector field of view. At the

Table 6
Measured geometrical parameters upon arrival to CET ('initial') and after adjustment ('adjusted'). Ideal alignment is given when x_D, y_D, θ, φ, and η are zero. The values for z_D and z_R do not have ideal values, yet their values in the backprojection step need to be consistent with their actual values. For this purpose, the accurate measurement of their quantity is critical.

Instrument alignment	Geometrical parameters						
	x_D/mm	y_D/mm	z_D/mm	z_R/mm	θ/°	φ/°	η/°
Initial	−0.1116	0.1498	−1208.6387	−398.4272	0.2329	0.0798	0.0092
Adjusted	0.0011	−0.0055	−1207.5453	−398.4683	0.0019	−0.0080	0.0117

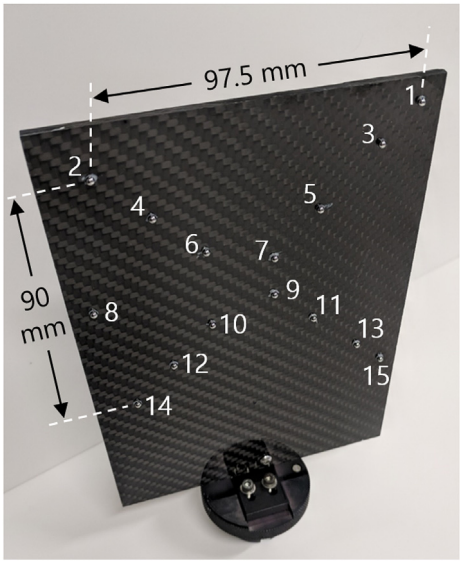

Fig. 14. The X-plate validation object.

$\alpha \approx 0°$ position, movement on the detector of sphere 6 is to the left (if facing the detector from the source), while the movement is to the right when the sphere is at the $\alpha \approx 180°$ position. The largest errors in vertical V pixel coordinate occur when the sphere movement is either towards or away from the detector, which nominally should correspond to the sphere 6 rotation positions $\alpha \approx 90°$ and $\alpha \approx 270°$. However, at these rotation positions, sphere 6 also experiences center projection errors of similar magnitude due to the uneven background intensities from the carbon fiber support. Therefore, the maxima and minima of V pixel coordinate errors for sphere 6 are offset to correspond to the superposition of blurring from the continuous sphere movement during the radiographic exposure and errors due to uneven background intensities (Fig. 12, bottom). Similar behaviors are observed for other spheres in the reference object.

The indexed rotation associated with a radiograph corresponds to the beginning of its exposure. Given a finite exposure, the acquired radiograph images the sphere as it moves from its position at the indexed rotation to its position at the end of the exposure. The acquired radiograph can therefore be considered an integral over many infinitesimally short exposures of the sphere as it moves away from its initial position at the beginning of the exposure, thereby resulting in a blurred image of the sphere (see Fig. 13, left for a magnified view of projected sphere 6 at its 180° position under each rotational speed). This blur is not symmetrical about the indexed angle associated with the exposure (Fig. 13, right), which results in an offset of the observed center projection coordinate from image analysis with respect to the modelled coordinate (which corresponds to the center projection at the beginning of the exposure). In fact, the discrepancy between the angle of rotation at the beginning of exposure and the continually moving sphere is indicated by the increase in solved reference object rotation position about the Y axis ρ_Y at the beginning of the scan, i.e. $\alpha = 0°$, with increased rotation speed (Table 5). Reducing the exposure time of the detector can theoretically reduce the effects of the moving sphere. However, the 1000 ms exposure time of the detector was not changed due to limitations in image buffering and transfer. Furthermore, shorter detector exposures reduce the signal-to-noise ratio.

7. Instrument adjustment

The output of the geometrical measurement procedure can be used to inform the alignment of the CT instrument by adjustment, i.e. mechanical re-positioning. Upon arrival on a second visit to CET, the geometry of the CT instrument was measured using 720 stepped projections of the CT^2 reference object. The output of this initial measurement is shown in Table 6. Given the measured misalignments, adjustments were made to the out-of-plane detector orientation (θ, φ) and lateral position (x_D, y_D) to bring the instrument to approximately ideal alignment. Lateral position was adjusted using the dedicated controllers, while detector out-of-plane rotations were adjusted by inserting washers between the detector frame and its mount (described in section 5). In-plane rotation was not intentionally adjusted since this misalignment is easily corrected in typical reconstruction software. Parameters z_D and z_R do not have dedicated aligned values, they need only be known accurately. The measured geometrical parameters after adjustment are also shown in Table 6.

To validate the performance of the output from the geometrical measurement procedure to inform the adjustment of the CT instrument, the X-plate validation object (Fig. 14) is CT measured in the initial and adjusted geometries. The X-plate consists of 15 grade 20 [10] chrome steel spheres of 2.5 mm diameter arranged in a dedicated manner on a carbon fiber plate. Sphere center positions in a local coordinate frame were measured by Nikon Altera CMM with a MPE of 2 + L/400 µm, where L is the measured length in mm. Acquisitions of 1440 projections of the X-plate are performed at the same sample stage position for which the instrument geometries were measured. The X-plate is reconstructed from initial and adjusted acquisitions with Inspect-X reconstruction software (Nikon Metrology). The values for SRD, source-to-detector distance (SDD), and voxel size in reconstruction of the initial dataset were set to the values estimated at CET using their procedure (see section 5). In the reconstruction of the adjusted dataset, SRD and SDD were set to the measured z_R and z_D, respectively, and the voxel size was calculated accordingly. Dual center of rotation estimation in Inspect-X is applied in reconstructions to estimate in-plane rotation and lateral position of the projected axis of rotation (approximately equivalent to the parameters η, x_D, and y_D in this study).

Discrepancies between SRD and SDD specified in the reconstruction metafile (used to define pre-weighting and backprojection geometry) and the effective SRD and SDD in the instrument can be partially corrected by implementing voxel rescaling [11]. Voxel rescaling factors are determined for each acquisition from center-to-center distance measurements on the nominally-reconstructed CT^2 from the same acquisition geometry. The scaling factors are 0.993839 and 0.999987 for initial and adjusted geometries, respectively. Applying voxel rescaling to the adjusted dataset did not produce significant differences to the CT measurements; therefore, these results are not presented. CT measurements of the X-plate from initial acquisition without and with voxel rescaling (henceforth 'initial' and 'rescaled', respectively) are compared

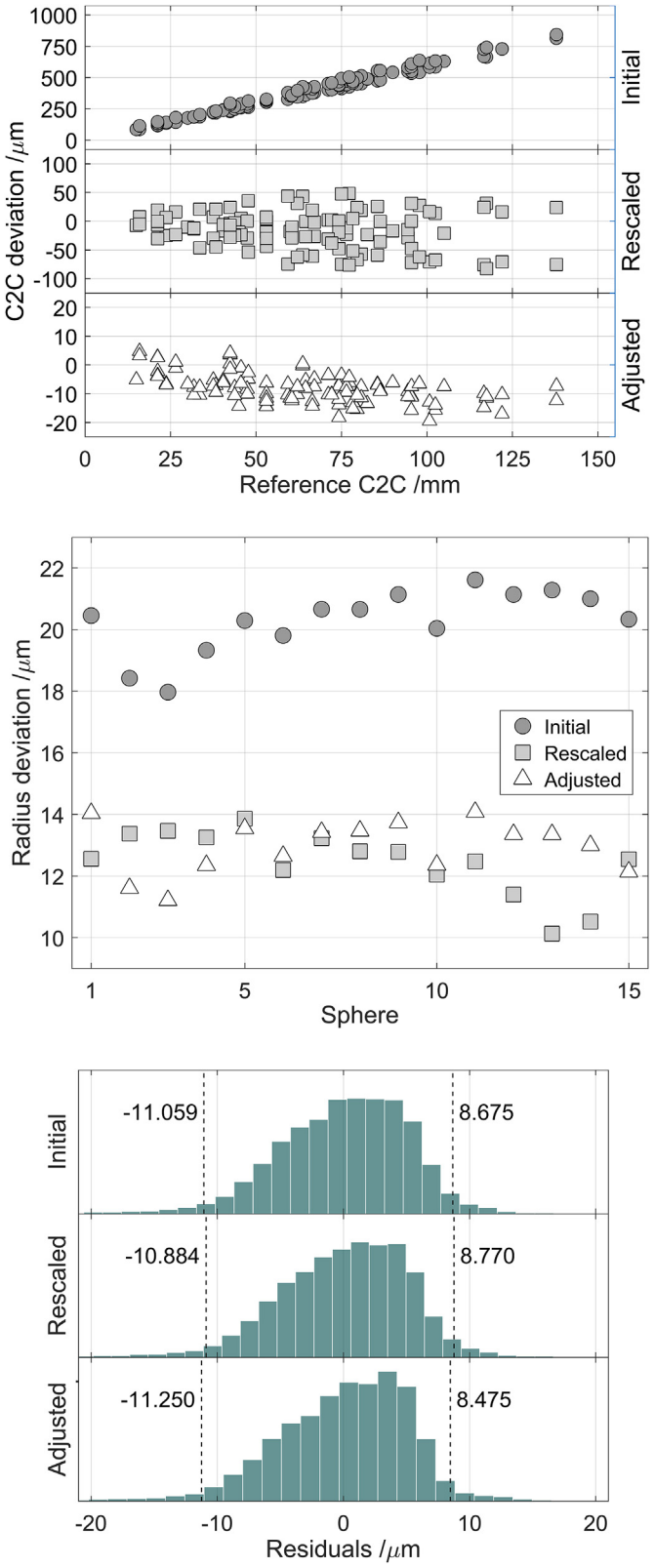

Fig. 15. Errors in measurement of sphere C2C distances between all combinations of sphere pairs (top), sphere radius (middle), and sphere form error illustrated as histograms of sphere fit residuals (bottom) in the reconstructed X-plate under initial, rescaled, and adjusted instrument geometries.

to the same CT measurements from the adjusted acquisition. The reconstructed three-dimensional grey value models are segmented into iso-surfaces by applying advanced local thresholding in VGStudio MAX 3.0 (Volume Graphics, GmbH). The iso-surfaces are converted to point clouds of three-dimensional surface coordinates by applying surface sampling at intervals of 1 voxel along each coordinate direction. The cloud of point coordinates is further analyzed in MATLAB (Mathworks, Inc). For each sphere in the reconstructed workpiece, a sphere is least-squares fit to the point coordinates belonging to the surface of that sphere. Sphere fit parameters are used to perform dimensional measurements on the reconstructed X-plate.

The distance between sphere fit centers is measured for all combinations of sphere pairs in nominal, rescaled, and adjusted reconstructed datasets and compared. Center-to-center distance (C2C) errors relative to the CMM measured reference distances are shown in Fig. 15 (top). As expected, rescaling removes length dependent errors, resulting in a reduction of maximum C2C errors from 843 μm in the initial dataset to approximately 82 μm in the rescaled dataset. Adjustment reduces the maximum C2C error to under 20 μm, which is approximately equal to the 23.6 μm diameter of the X-ray source focal spot for the settings used. Sphere fit radius errors relative to the nominal radius are presented in Fig. 15 (middle). Rescaling reduces sphere fit radius errors from initial dataset by approximately 7 μm, from approximately 20 μm to approximately 13 μm. While the magnitude of sphere fit radius errors were not significantly changed after adjustment, the variation in errors was reduced from 3.64 μm and 3.73 μm in initial and rescaled datasets, respectively, to 2.87 μm in the adjusted dataset. Reconstructed sphere form is presented in Fig. 15 (bottom) as the distribution of sphere fit residuals over all spheres in histogram form. Vertical dashed lines are the 2.5% and 97.5% quantiles, corresponding to the lower and upper boundaries, respectively, of 95% of the sphere fit residuals. Differences in sphere fit residuals are very small among datasets. This outcome is expected as it was shown in Ref. [12] that a tilt θ of the detector (the largest angular misalignment in the initial instrument) does not significantly affect sphere form.

8. Conclusion

In this study, we apply a procedure for CT geometry measurement on an experimental instrument. The measured geometry is only valid for the sample stage position in which the procedure is performed due to kinematic error motions in sample stage positioning. The development of an integrated geometrical mapping procedure for the entire CT measurement range is a topic of future work. The robustness of the measurement procedure is tested with respect to the number of acquired stepped projections and the mode with which the reference object is rotated. The variation in solved parameter values from the various acquisitions of stepped projections were small. The largest deviations in solved parameter values occurred for acquisitions of less than 5 stepped projections. Reprojection errors from continuous rotation were overall larger than the reprojection errors from stepped rotation and increased with increasing rotation speed. Solved parameters from continuous rotation acquisition exhibited the largest relative deviations in detector horizontal position x_D and in-plane rotation η.

The output from the geometrical measurement procedure is used to inform the physical adjustment of the experimental CT instrument to the ideal alignment as defined for typical FDK-type reconstruction algorithms. Results from the reconstructed datasets after adjustment indicate an overall reduction of dimensional measurement errors for the X-plate validation object. Sphere center to center distances were reduced from a maximum of approximately 840 μm and 82 μm in initial and rescaled datasets, respectively, to less than 20 μm after adjustment. This reduced error is approximately equal to the diameter of the X-ray focal spot for the source settings used here. These results shed light on the ineffectiveness of voxel rescaling in compensating geometrical misalignments of the CT instrument. Sphere radius errors were reduced by 7 μm after voxel rescaling; adjustment did not provide significant improvements to the magnitude of these errors after rescaling. However, variation in sphere radius errors among all spheres was

reduced from 3.73 µm in the rescaled dataset to 2.87 µm after adjustment. Sphere form, presented as the distribution of sphere fit residuals, was not significantly improved by either rescaling or adjustment. This observation is consistent with previous findings [12], which indicate that detector tilt θ (the largest angular misalignment in the initial instrument geometry) does not significantly affect sphere form.

The results presented in this study indicate the robustness of the proposed procedure to measure the geometry of a CT instrument. The measured geometrical parameters were used to adjust the instrument to the ideal configuration as defined in the tomographic reconstruction algorithm. Reductions in observed dimensional errors on a separate validation object after adjustment serve as experimental validation of the effectiveness in the proposed procedure.

Acknowledgments

The research presented here was made possible by funding from the European Union FP7 MSCA ITN INTERAQ*CT* project (grant agreement 607817), from the Belgian American Educational Foundation, from the European Union Horizon 2020 MSCA Individual Fellowship FlexCT (grant agreement 752672), and from the European Regional Development Fund in frame of the project Com3D-XCT (ATCZ-0038) in the Interreg V-A Austria - Czech Republic program.

References

[1] Ferrucci M. Towards traceability of CT dimensional measurements. In: Carmignato S, Dewulf W, Leach RK, editors. Ind. X-ray comput. Tomogr. Berlin, Germany: Springer-Verlag; 2017.

[2] Ferrucci M, Leach RK, Giusca CL, Carmignato S, Dewulf W. Towards geometrical calibration of X-ray computed tomography systems - a review. Meas Sci Technol 2015;26:92003. http://dx.doi.org/10.1088/0957-0233/26/9/092003.

[3] Fíla T, Vavřík DEP. 2835631 B1 A multi-axial apparatus for carrying out x-ray measurements, particularly computed tomography. 2016.

[4] Hermanek P, Ferrucci M, Dewulf W, Carmignato S. Optimized reference object for assessment of computed tomography instrument geometry. 7th conf. ind. comput. tomogr. 2017. p. 7–8.

[5] Ferrucci M, Hermanek P, Ametova E, Carmignato S, Dewulf W. Measurement of the X-ray computed tomography instrument geometry by minimization of reprojection errors—implementation on simulated data. Precis Eng n.d.; In press, accepted.

[6] Deng L, Xi X, Li L, Han Y, Yan B. A method to determine the detector locations of the cone-beam projection of the balls' centers. Phys Med Biol 2015;60:9295–311. http://dx.doi.org/10.1088/0031-9155/60/24/9295.

[7] Mathworks. Global search class. 2010.

[8] Kwan ALC, Seibert JA, Boone JM. An improved method for flat-field correction of flat panel x-ray detector.pdf. Med Phys 2006;33.

[9] Claus BEH. Geometry calibration phantom design for 3D imaging. Proc SPIE 2006;6142. http://dx.doi.org/10.1117/12.652342. 61422E–61422E–12.

[10] ISO 3290-1 rolling bearings - balls - steel balls. International Organization for Standardization; 2014.

[11] Stolfi A, De Chiffre L. 3D artefact for concurrent scale calibration in Computed Tomography. CIRP Ann - Manuf Technol 2016;65:499–502. http://dx.doi.org/10.1016/j.cirp.2016.04.069.

[12] Ferrucci M, Ametova E, Carmignato S, Dewulf W. Evaluating the effects of detector angular misalignments on simulated computed tomography data. Precis Eng 2015:1–12. http://dx.doi.org/10.1016/j.precisioneng.2016.03.001.